Catalysis Today 146 (2009) 15–19

Contents lists available at ScienceDirect

Catalysis Today

journal homepage: www.elsevier.com/locate/cattod

Platinum–antimony tin oxide nanoparticle as cathode catalyst for direct methanol fuel cell

Dae Jong You, Kyungjung Kwon, Chanho Pak *, Hyuk Chang

Energy Group, Emerging Center, Corporate Technology Operations SAIT, Samsung Electronics Co., Ltd., San #14-1, Nongseo-dong, Giheung-gu, Yongin-si, Gyeonggi-do 446-712, Republic of Korea

ARTICLE INFO

Article history:
Available online 20 January 2009

Keywords:
Platinum
Antimony tin oxide
Cathode catalyst
Oxygen reduction reaction
Methanol tolerant catalyst
Direct methanol fuel cell

ABSTRACT

Pt–ATO (Sb/SnO_2) nanoparticle is synthesized by the consecutive polyol process to enhance the catalyst activity for the oxygen reduction reaction (ORR) in the presence of methanol. Pt–ATO catalyst exhibits better activity for ORR with and without methanol than Pt black catalyst in a half-cell test, which could be attributed to the inhibition of the coagulation of Pt nanoparticles and partial blocking of adsorption site for the methanol molecules by ATO particle on the Pt surface. As a result, an increase in the power density in the single cell test was achieved by using the Pt–ATO catalyst as cathode catalyst for the direct methanol fuel cell (DMFC) rather than by using the Pt black catalyst. The Pt–ATO particle appears to be promising methanol tolerant catalyst with higher activity for the ORR in the DMFC.

1. Introduction

Direct methanol fuel cell (DMFC) is attracting much attention as an alternative potential power source for next generation portable electronic devices due to its high energy density, feasible operation conditions at ambient temperature, and easy availability of liquid fuel [1,2]. However, there still remain challenging research issues for the commercialization of DMFC for the portable power source market. One of the important issues is to develop a new structural and compositional cathode catalyst having a higher activity for the oxygen reduction reaction (ORR) and a lower activity for the methanol oxidation reaction (MOR) caused by methanol crossover from the anode to the cathode through polymer electrolyte membranes, leading to a potential loss of 50 mV at 100 mA cm^{-2} and reduction in efficiency by 25% at relatively low temperature [3].

To overcome this issue, considerable researches have been made in exploiting a sufficiently selective and active electrocatalyst for the DMFC cathode. One approach is to use Pt metal alloys with various transition metals (Cr, Fe, Co, Ni, etc.) that are believed to produce favorable effects on the ORR. These effects are the structural effect for shortening the Pt–Pt distance in the alloy nanoparticles and weakening the Pt–oxygen bond, the electrochemical effect for enhancing the electron transfer from oxygen to Pt, and the blocking effect for preventing the adsorption of methanol on Pt atom around the transition metal [4]. However, the transition metal in the alloy catalyst is easily leached out electrochemically in acidic aqueous solution because the segregation and oxidation of transition metal at the surface of the Pt occurs during the preparation of these alloy catalysts [5,6]. In addition, Pt-based transition metal alloy catalyst is commonly heat-treated at a high temperature to suppress the segregation and oxidation problem, which gives rise to undesired sintering of metal nanoparticles [7]. Consequently, the intrinsic catalytic activity of Pt-based transition metal alloy catalyst towards the ORR and the durability under the fuel-cell operating condition are lower than those of Pt catalyst.

Another approach is to use non-noble metal electrocatalysts based on chalcogenides and macrocycles of transition metals. Although the oxidation of methanol on the cathode is greatly avoided with these catalysts, these materials are far from reaching the catalytic activity of Pt [8,9]. Very recently, Cho et al. [10] reported that the supported Pt/C catalyst in the cathode of the DMFC can improve the methanol tolerance. Thus, the development of novel supported catalyst using advanced carbon support [11,12] is one of the feasible candidates for mitigating the methanol crossover in the DMFC.

In this study, Pt nanoparticle contacting with adjacent ATO was prepared by a consecutive polyol process with aiming to the high activity for the ORR and the methanol tolerant selectivity. ATO enables the adsorption of OH species to occur at a low potential, which promotes the electro-oxidation of CO and low molecular

* Corresponding author. Tel.: +82 31 280 6884; fax: +82 31 280 9359.
E-mail address: chanho.pak@samsung.com (C. Pak).

0920-5861/$ – see front matter © 2008 Elsevier B.V. All rights reserved.
doi:10.1016/j.cattod.2008.12.004

alcohol, such as methanol and ethanol as suggested in recent studies [13,14]. Feasibility of using this catalyst for cathode is demonstrated in the single cell of DMFC.

2. Experimental

2.1. Synthesis of Pt–ATO nanoparticles

A polyol method is a kind of unprotected colloid method with the advantages of both impregnation [15] and protected colloid procedure [16], such as the simplicity of preparation, the narrow distribution of prepared particles, and the easy control of particle size. Synthesis parameters such as pH, the ratio of water to ethylene glycol (EG), the total amount of reaction mixture solvent, and the molar ratio of ATO to Pt were optimized through the design of experiment approach.

If the pH value was lower than 11, Pt colloid particle was not generated in the solution during the heating process in the polyol process. The role of water in EG solution is believed to help to retard the nucleus formation rate of the particles, and control the size of the metal nanoparticles [17]. The amount of total solvent should have influence on the growth and aggregation of Pt colloid. Furthermore, the variation of the Pt/ATO molar ratio could affect the number of catalyst active site related to the ORR and the MOR.

The consecutive polyol process for the Pt–ATO catalyst consists of the following procedures: 2.36 g of $H_2PtCl_6{\cdot}xH_2O$ (Umicore, 39.8 wt.% Pt) was dissolved in 197.4 g of EG, and then subsequently the pH of the solution was adjusted to about 11 using 0.2 M NaOH solution. The temperature of the mixture was ramped up to 383 K over 1 h, and kept for 2 h to produce the Pt colloidal solution, and then cooled down to room temperature (RT). Refluxing conditions were used in order to maintain water contents in the mixture. Continuously, Pt nanoparticles with neighboring ATO nanoparticles were formed by repeating the above reduction step after adding quarter gram of tin chloride ($SnCl_2{\cdot}2H_2O$, Aldrich) and 0.03 g of antimony chloride ($SbCl_3$, Aldrich) to the preformed Pt colloidal solution. The resulting catalyst, Pt–ATO nanoparticles, was filtered, washed with deionized (DI) water, and finally freeze–dried.

2.2. Preparation of membrane–electrode assembly (MEA)

EG (98%, Aldrich) and Nafion® PFSA polymer dispersion (20 wt.%, DuPont) were used as received. PtRu black (HiSpec 6000) purchased from Johnson Matthey and in-house Pt–ATO was used as the anode and cathode catalysts, respectively. Pt black (HiSpec 1000) was also used as cathode catalysts for the comparison. The conductivity and the thickness of Nafion-115 membrane used in this study was 0.1 S cm^{-1} and 100 μm, respectively.

Catalyst inks, consisting of the catalysts, Nafion® solution, DI water, and EG were well dispersed by using the high speed rotating equipment (conditioning mixer, AR-500) for 10 min. To prepare the catalyst layers, the catalyst inks were uniformly coated onto polyethylene terephthalate (PET) blank films to give a metal loading of about 5 mg cm^{-2} for both anode and cathode. And then, these were dried for 24 h in a vacuum oven at 393 K. The catalyst coated membrane (CCM) was obtained using the decal transfer method by which the catalyst layer of both anode and cathode transferred from the PET films to the Nafion® 115 membrane by hot pressing. The CCM was pre-treated in the mixture of 1 M methanol and 1 M sulfuric acid solution at 368 K for 4 h to activate the membrane and catalyst layer. Finally, the MEA was formed by placing the anode and cathode diffusion layer onto the corresponding sides of the CCM by hot pressing.

2.3. Characterization

The X-ray diffraction (XRD) patterns were obtained by Philips X'pert Pro X-ray diffractometer equipped with a Cu-K_α source at 40 kV and 40 mA. The crystalline size of Pt–ATO nanoparticle and Pt black catalyst was calculated from Scherrer's equation using XRD patterns [18]. Transmission electron microscopy (TEM) images were obtained by using G2 FE-TEM Tecnai microscope at an accelerating voltage of 200 kV. A 50 mg of Pt–ATO sample was decomposed in a mixture of 5 ml of DI water, 4.75 ml of 35 wt.% HCl, 0.2 ml of 50 wt.% HF and 0.10 ml of 70 wt.% HNO_3 with HP500 high-pressure microwave digestion vessel system (CEM) at 450 K and 170 psi. The composition of Pt, Sb and Sn was determined by ICP-AES on Shimadzu ICPS-8100 sequential spectrometer. The composition of oxygen was determined by subtracting the calculated amount by ICP result from the initial amount of Pt–ATO catalyst.

X-ray photoelectron spectroscopy (XPS) was performed by using AXIS (Q2000) photoelectron spectrometer. The X-ray source was mono-Al-K_α operating at 1486.6 eV. The N_2 adsorption measurements were made for the catalyst powders of Pt–ATO and Pt black using a TRISTAR-3000 (Micromeritics) and the BET surface area and the pore volumes were calculated as described earlier [11].

Electrochemical characterization was performed with Solartron Potentiostat (Model SI 1287). A standard three-electrode electrochemical cell was used. A Pt mesh and a KCl-saturated Ag/AgCl electrode were served as the counter and the reference electrode, respectively. The working electrode was prepared by brushing the same catalyst ink for CCM preparation on a carbon paper (Toray-060 plain). All electrode potentials in this paper were converted to normal hydrogen electrode (NHE).

Cyclic voltammogram for the electrochemical surface area (ESA) was recorded in the potential range of 0.05–1.4 V versus NHE at a scan rate of 5 mV s^{-1} after the cycling 20 mV s^{-1} in 0.1 M $HClO_4$ solution at RT, which was saturated with nitrogen by bubbling pure nitrogen for 30 min.

The linear scan voltammetry for the ORR was obtained at a scan rate of 1 mV s^{-1} at RT, which was saturated with oxygen by bubbling pure oxygen gas for 30 min with and without 0.1 M MeOH solution.

The performance of the single cell MEA was evaluated by measuring the current density versus the cell voltage with a commercial fuel-cell test system (Wonatech). The polarization curves were obtained in the voltage range from open circuit voltage (OCV) to 0.2 V at 323 K with circulating 1 M methanol through the anode at a rate of 0.3 ml $(min\ A)^{-1}$ and feeding air to the cathode at a rate of 52.5 ml $(min\ A)^{-1}$.

3. Results and discussion

3.1. Physicochemical characterization of Pt–ATO catalyst

XPS was used to determine the surface oxidation states of the components in the Pt–ATO nanoparticles. Table 1 shows the

Table 1
The binding energies of Pt $4f^{7/2}$ and Sn $3d^{5/2}$ in the XPS spectra from Pt–ATO and Pt black catalysts.

	Pt $4f^{7/2}$			Sn $3d^{5/2}$	
	PtO_2	PtO	Pt	SnO_2	Sn
In the literatures[a]	74.5	72.9	71.6	486.9	485.3
Pt–ATO	–	–	71.5	487.0	–
Pt black	–	–	71.5	–	–

[a] Refer to Refs. [19,28].

position of peak for the $4f^{7/2}$ of Pt and $3d^{5/2}$ of Sn regions of the XPS spectra of the Pt–ATO and Pt black catalysts. The most intense doublets of $4f^{7/2}$ of Pt at 71.5 eV and $3d^{5/2}$ of Sn at 487 eV could be assigned to metallic Pt and tin oxide (SnO_2), respectively, according to the previous report [19]. It is indicated that Pt and Sn atoms hardly interdiffused to form Pt–Sn alloy or Pt–Sn–O complexes at the Pt–ATO interface during the synthesis. A slight shift from the value (70.9 eV) of bulk Pt to higher binding energy is a known effect for small nanoparticles, as reported by Roth et al. [19]. Thus, this result clearly shows that ATO nanoparticles formed adjacent to Pt nanoparticles in EG solution.

The chemical composition of Pt–ATO nanoparticle measured by ICP-AES catalyst is listed in Table 2. The final composition is almost the same as that on an input basis. The molar ratio of Sb to Sn is 1/10, which is known ratio to show the highest electrical conductivity owing to the presence of Sb in two oxidation states, namely Sb^{5+} and Sb^{3+} [20]. The molar ratio of ATO to Pt is 1/4, which could support the assumption that the configuration of Pt–ATO such as one ATO molecule around four Pt atoms should affect the ORR and MOR activity of Pt. This issue will be discussed in detail later.

Fig. 1 shows representative X-ray diffraction patterns for Pt–ATO and Pt black catalysts. Both samples are identified as a face-centered cubic structure with the similar lattice parameters of 0.3945 and 0.3983 nm, respectively, which could be evidenced that most ATO formed as a separate phase in the vicinity of Pt rather than exists in the interstitial sites of Pt crystal lattice. The crystalline size by using the Scherrer's equation [18] from the XRD patterns at Pt (1 1 1) plane of Pt–ATO catalyst (about 3.5 nm) is smaller than that of Pt black (about 7.9 nm). The modification of Pt with ATO prevents the Pt nanoparticles from aggregation, which contributes to the small particle size. No phase ascribed to ATO compound can be seen in the XRD pattern, possibly due to its smaller amount relative to Pt. However, an increase in atomic ratio of ATO to Pt could enhance ATO peak appearing in a typical polycrystalline diffraction pattern of cassiterite in which some antimony atoms are doped into the substitution sites of SnO_2 [21].

Table 2
Chemical composition of Pt–ATO catalyst measured by ICP-AES.

	Element			
	Pt	Sn	Sb	Oxygen
wt.%	76.5	10.7	1.3	11.5
Mole	0.40	0.09	0.01	0.72

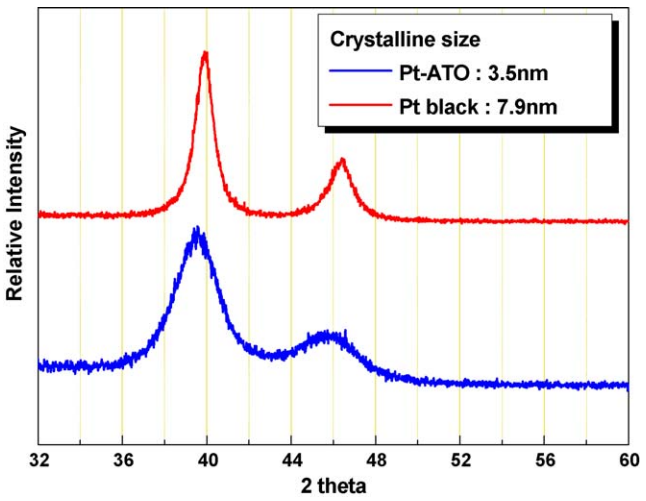

Fig. 1. XRD patterns of Pt–ATO and Pt black catalysts.

To investigate the morphology of Pt particles in the Pt–ATO and Pt black catalyst, TEM images were obtained as in Fig. 2. While agglomerates of Pt nanoparticles are observed in the Pt black catalyst, the spherical Pt–ATO catalyst is uniformly dispersed without agglomeration of nanoparticles, which indicates that the addition of ATO to the Pt colloidal particles could prevent the coagulation of Pt nanoparticles. When hundred particles in a random region are sampled, the average particle size of Pt–ATO is estimated to be 2.5 nm, whereas the particle size of Pt is estimated to be 10.2 nm.

The BET surface area and total pore volume of the Pt–ATO and Pt black catalysts were estimated by N_2 adsorption method and summarized in Table 3. The Pt–ATO catalyst exhibited twice higher surface area and total pore volume than Pt black catalyst, which is in accordance with the result of TEM image and XRD result.

3.2. Electrochemical characterization of Pt–ATO catalyst

Fig. 3 shows characteristic cyclic voltammograms of Pt–ATO and Pt black catalysts. All samples exhibit hydrogen adsorption/

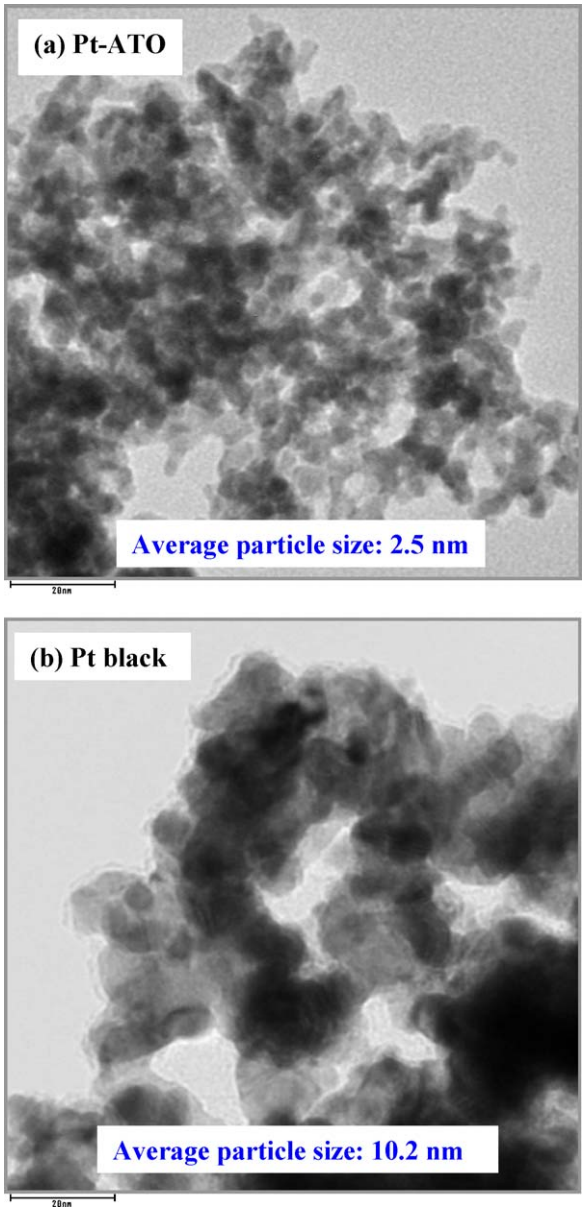

Fig. 2. TEM micrograph of the Pt–ATO and Pt black catalysts. Magnification: 200 K.

Table 3
BET surface area and total pore volume estimated from N_2 adsorption of the Pt–ATO and Pt black catalyst.

Sample	BET surface area ($m^2\ g^{-1}$)	Total pore volume ($cm^3\ g^{-1}$)
Pt–ATO	60	0.31
Pt black	29	0.12

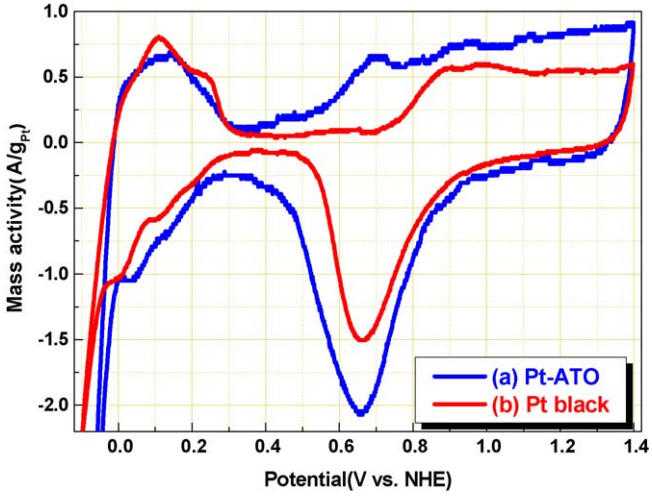

Fig. 3. Cyclic voltammograms of the Pt–ATO and Pt black catalysts in N_2-saturated 0.1 M $HClO_4$ at a sweep rate of 5 mV s^{-1} and room temperature.

desorption peak at 0.05–0.3 V and Pt-oxide formation/reduction peak at 0.8–1.4 V. The ESA calculated from H-desorption area of Pt–ATO is almost the same as that of Pt black (15 m^2/g_{Pt}). The discrepancy between surface area by BET equation using N_2 adsorption isotherm and ESAs from CV might result from the fact that the well-defined hydrogen adsorption/desorption behavior at Pt is disturbed by other faradaic processes [22]. Dassenoy et al. reported that the coverage of the ruthenium surface by selenium allows enough free active sites for an efficient electrocatalysis or coordination with oxygen/water, but this structure of RuSe catalyst is completely suppressed at the hydrogen desorption peak [23]. The oxidation current peak at 0.8–1.4 V of Pt–ATO catalyst is much higher than that of Pt black, which is in accord with the structural effect reported by Dassenoy et al.

Fig. 4 displays the ORR polarization curves for Pt–ATO and Pt black catalysts in O_2-saturated 0.1 M $HClO_4$ solution at RT. Both curves illustrate the typical polarization behavior for the electrochemical reduction of molecular oxygen with the current starting to flow above 0.9 V. The ORR mass activity of the Pt–ATO catalyst measured at 0.8 V is 1.7 times higher than that of the Pt black catalyst. The inset in Fig. 4 shows the Tafel slopes of the two catalysts above 0.8 V. It seems an inflection point around 0.83 V for both catalysts and the Tafel slope in the potential range above 0.83 V is about 80 mV dec^{-1}, which is a similar value of Pt catalyst in acid electrolyte [24]. Although the slope in the range from 0.8 V to 0.83 V is higher than 80 mV dec^{-1}, we compare the ORR mass activity at 0.8 V for the sake of convenience. The same Tafel slopes of both catalysts prove that the addition of ATO did not change the ORR mechanism of Pt substantially. Therefore, the higher ORR mass activity of Pt–ATO can be attributed to the smaller particle size of Pt with ATO than Pt alone.

The methanol tolerant properties of the catalysts were examined by polarization experiments in an O_2-saturated 0.1 M $HClO_4$ solution containing 0.1 M methanol as shown in Fig. 5. Although the ORR polarization curve of the Pt–ATO catalyst in Fig. 5(a) is not greatly changed in the presence of methanol, that of the Pt black catalyst in Fig. 4(b) has two signs of ongoing methanol oxidation reaction as a side reaction. The hump around 0.75 V and the oxidation current at more than 0.9 V result from methanol oxidation, and these characteristic current can be magnified in a more concentrated methanol solution. The more methanol-tolerant behavior of Pt–ATO catalyst could be explained by the geometric "ensemble" effect [25,26]. It is well known that the dissociative chemisorption of methanol requires the existence of several adjacent Pt ensembles. Therefore, the presence of atoms of the second metal or metal oxide around Pt active sites could block methanol adsorption on Pt sites due to the ensemble effect. Consequently, methanol oxidation on the binary component electrocatalyst can be suppressed. On the other hand, the dissociative chemisorption of oxygen, requires only two adjacent Pt sites, and is less affected by the presence of the second metal or metal oxide. The composition of Pt–ATO catalyst, one ATO molecule with four Pt atoms as mentioned in Section 3.1, results in a low activity towards methanol oxidation, and thus, a high methanol tolerance during the ORR.

An MEA was prepared using the Pt–ATO nanoparticle as cathode catalyst, and comparison of its performance with an MEA using the Pt black catalyst is shown in Fig. 6. The cell voltage of Pt–ATO in the range of 1–10 mA cm^{-2} (refer to the inset in Fig. 6), which is mainly related to region of catalytic activity and low potential loss of methanol crossover for the DMFC [27], is higher

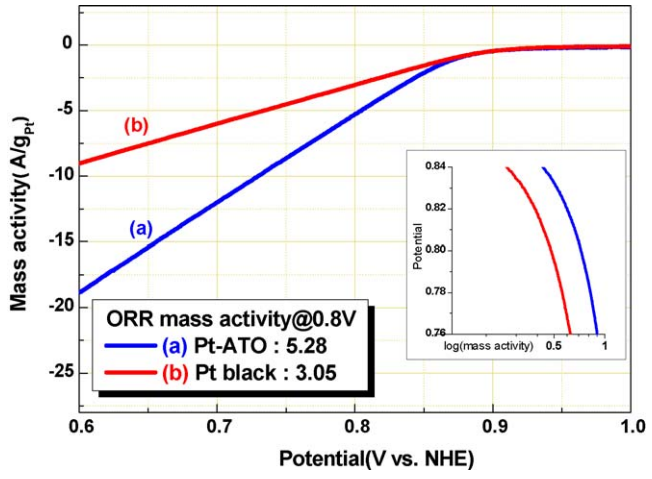

Fig. 4. Polarization curves for the ORR on the Pt–ATO and Pt black catalyst in O_2-saturated 0.1 M $HClO_4$ at a sweep rate of 1 mV s^{-1} and room temperature.

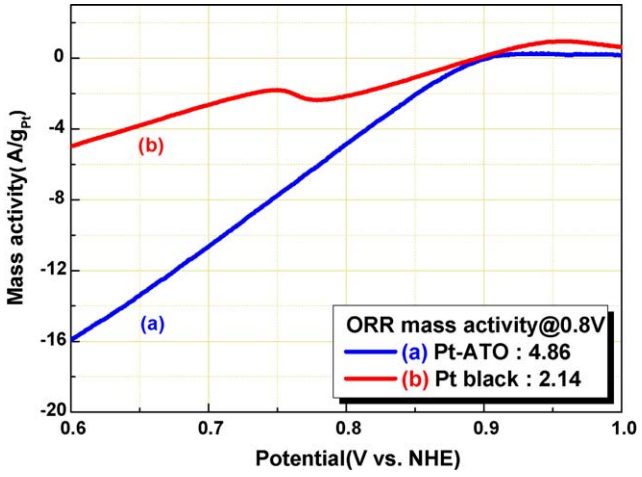

Fig. 5. Polarization curves for the ORR on the Pt–ATO and Pt black catalyst in O_2-saturated 0.1 M $HClO_4$ containing 0.1 M CH_3OH at a sweep rate of 1 mV s^{-1} and room temperature.

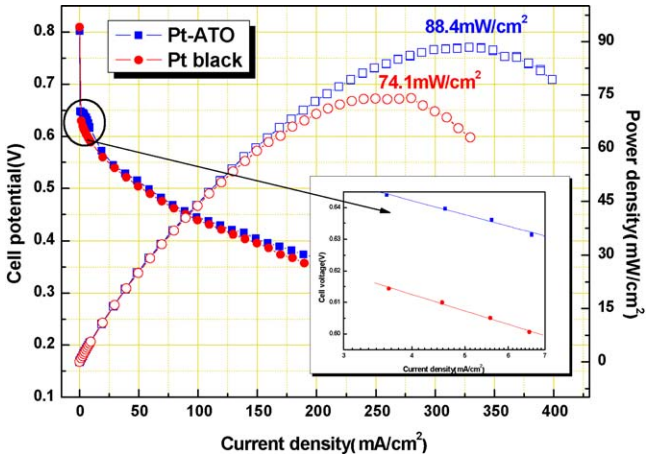

Fig. 6. The polarization curve of the single cell MEA having Pt–ATO and Pt black catalysts as the cathode catalysts. The counter anode catalyst is PtRu black and the active area of MEA is 10 cm^2.

than that of Pt black catalyst. This is in agreement with the above result from the ORR test with and without methanol. Thus, the maximum power density is 88.4 mW cm^{-2} for Pt–ATO catalyst and 74.1 mW cm^{-2} for Pt black catalyst, respectively. As a result, this can be attributed to the enhanced ORR activity by the larger catalytic surface area and the better methanol tolerance by the blocking of ATO nanoparticles nearby to Pt surface, in agreement with the half-cell results.

4. Conclusion

Pt–ATO nanoparticles comprising of Pt nanoparticles with adjacent ATO are synthesized using the stepwise polyol method. According to the XPS study, Pt exists as a metal phase and ATO exists as a metal oxide phase without alloying each other. From the TEM and XRD analysis, the particle size of Pt–ATO catalyst (about 3.5 nm) is smaller than that of Pt black (about 7.9 nm). Relatively small Pt particles are formed with the addition of ATO because nanoscale ATO nanoparticles can inhibit the agglomeration of Pt nanoparticles during the synthesis.

The Pt–ATO catalyst shows improved electrochemical activities for the ORR compared with the Pt black catalyst in both half-cell and single cell tests regardless of methanol. The methanol tolerant property of Pt–ATO catalyst is attributed to the blocking effect of ATO on the surface of Pt–ATO nanoparticles. The higher ORR activity and the methanol tolerant property of the Pt–ATO catalyst make this material a suitable cathode catalyst for the application in the DMFC. Also, the consecutive polyol method can be used to prepare other core-shell structured catalysts.

References

[1] M. Neergat, D. Leveratto, U. Stimming, Fuel Cells 2 (2002) 1615.
[2] H. Chang, S.H. Joo, C. Pak, J. Mater. Chem 17 (2007) 3078.
[3] X. Ren, P. Zelenay, S. Thomas, J. Davey, S. Gottesfeld, J. Power Sources 86 (2000) 111.
[4] W. Yuan, K. Scott, H. Cheng, J. Power Sources 163 (2006) 323.
[5] A.K. Shukla, M. Neergat, P. Bera, V. Jayaram, M.S. Hegde, J. Electroanal. Chem. 504 (2001) 111.
[6] K. Park, J. Choi, B. Kwon, S. Lee, Y. Sung, H. Ha, S. Hong, H. Kim, A. Wieckowski, J. Phys. Chem. B 106 (2002) 1869.
[7] E. Antolini, Mater. Chem. Phys. 78 (2003) 563.
[8] D. Cao, A. Wieckowski, J. Inukai, N. Alonso-Vante, J. Electrochem. Soc. 153 (2006) 869.
[9] F. Charreteur, S. Ruggeri, F. Jaouen, J.P. Dodelet, Electrochim. Acta 53 (2008) 6881.
[10] Y.-H. Cho, H.-S. Park, Y.-H. Cho, I.-S. Park, Y.-E. Sung, Electrochim. Acta 58 (2008) 5909.
[11] S.H. Joo, C. Pak, D.J. You, S.-A. Lee, H.I. Lee, J.M. Kim, H. Chang, D. Seung, Electrochim. Acta 52 (2006) 1618.
[12] H.I. Lee, J.H. Kim, D.J. You, J.E. Lee, J.M. Kim, W.-S. Ahn, C. Pak, S.H. Joo, H. Chang, D. Seung, Adv. Mater. 20 (2008) 757.
[13] K.S. Lee, I.S. Park, Y.H. Cho, D.S. Jung, N. Jung, H.Y. Park, Y.E. Sung, J. Catal. 258 (2008) 143.
[14] H. Chhina, S. Campbell, O. Kesler, J. Power Sources 161 (2006) 893.
[15] A.S. Aricò, Z. Poltarzewski, H. Kim, A. Morana, N. Giordano, V. Antonucci, J. Power Sources 55 (1995) 159.
[16] H. Bönnemann, W. Brijoux, R. Brinkmann, E. Dinjus, T. Joussen, U.B. Korall, Angew. Chem. Int. Ed. 30 (1991) 1312.
[17] (a) Y. Wang, J. Ren, K. Deng, L. Gui, Y. Tang, Chem. Mater. 12 (2000) 1622; (b) D.J. You, S.-A. Lee, S.H. Joo, C. Pak, H. Chag, D. Seung, Stud. Surf. Sci. Catal 162 (2006) 537.
[18] S.S. Mao, G. Mao, US Patent 6,686,308 B2 (2004).
[19] C. Roth, M. Goetz, H. Fuess, J. Appl. Electrochem. 31 (2001) 793.
[20] M. Kojima, H. Kato, M. Gatto, Philos. Mag. B 68 (1993) 215.
[21] H.-J. Ahn, H.-C. Choi, K.-W. Park, S.-B. Kim, Y.-E. Sung, J. Phys. Chem. B 108 (2004) 9815.
[22] F.C. Nart, W. Vielstich, in: W. Vielstich, A. Lamm, H.A. Gasteiger (Eds.), Handbook of Fuel Cells, vol. 2, Wiley, West Sussex, 2003 (Chapter 21).
[23] F. Dassenoy, W. Vogel, N. Alonso-Vante, J. Phys. Chem. B 106 (2002) 12152.
[24] H.A. Gasteiger, S.S. Kocha, B. Sompalli, F.T. Wagner, Appl. Catal. B 56 (2005) 9.
[25] C. Lamy, A. Lima, V. Le Rhun, C. Coutanceau, J.M. Leger, J. Power Sources 105 (2002) 283.
[26] H.A. Gasteiger, N.M. Markovic, P.N. Ross, E.J. Cairns, Electrochim. Acta 39 (1994) 1825.
[27] M.P. Hogarth, T.R. Ralph, Platinum Met. Rev. 46 (2002) 146.
[28] A.K. Shukla, A.S. Aricò, K.M.E. Khatib, H. Kim, P.L. Antonucci, V. Antonucci, Appl. Surf. Sci. 137 (1999) 20.